Int. J. Heat Mass Transfer. Vol. 31, No. 2, pp. 321–330, 1988
Printed in Great Britain

0017–9310/88 $3.00 + 0.00

Freezing of saturated and superheated liquid in porous media

S. CHELLAIAH and R. VISKANTA
Heat Transfer Laboratory, School of Mechanical Engineering, Purdue University, West Lafayette, IN 47907, U.S.A.

(*Received* 1 *September* 1987)

Abstract—Freezing of saturated and superheated liquid-porous media contained in a rectangular test cell has been studied experimentally. Water and different diameter glass beads constituted the liquid and porous media, respectively. The effects of different size glass beads, imposed temperature difference and liquid superheat were investigated. A one-dimensional conduction-based model was used to examine the importance of non-equilibrium effects. These effects were found to be unimportant for both water–aluminum balls and water–glass bead systems. For water initially at the freezing temperature, the model predictions agreed well with the experimental temperature and solidification front position data. When the superheat was sufficiently high to induce buoyancy driven convective flow, the local freezing rates varied with vertical location along the cooled wall. For low superheat, due to the density inversion of water, the rate of freezing at the top was higher than at the bottom; however, for large superheat, the freezing rate near the bottom was higher as in freezing of ordinary liquids.

INTRODUCTION

FREEZING of liquid saturated porous media occurs in nature and in many engineering systems. Some of the specific applications include freezing of soil [1], freeze drying of food stuffs [2], and latent heat-of-fusion energy storage [3]. Artificial freezing of the ground is used as a structural support and as a water barrier for construction and mining purposes [4]. The prediction of the performance of ground-based heat pumps that use heat exchanger pipes buried underground [5, 6] depends on a thorough understanding of the freezing and thawing of the soil. In spite of numerous important technological applications, relatively little research attention has been given to the study of solid/liquid phase change of liquid saturated porous media [7]. The related problem of natural convection in porous media in the absence of phase change has been investigated both experimentally and numerically by many researchers and up-to-date reviews are available [8, 9].

Goldstein and Reid [10] studied the phase change of a water-saturated porous medium in the presence of a seepage flow. The analytical solution was based on the complex variable theory. Using this method, the energy equation in the unfrozen region can be solved without knowing the shape of the frozen region. Results are presented to show how the fluid flow affects the shape and growth rate of the frozen region embedded in the porous media. The finite element method was used by Hashemi and Sliepcevich [11] to model the freezing around a row of pipes in the presence of groundwater flow normal to the pipe centerline. They used the same energy equation for the solid and the liquid and accounted for latent heat effects in the temperature dependent specific heat over a suitable temperature range. A similar analysis was developed by Frivik and Comini [12] to model the freezing and thawing of soils in the presence of a seepage stream. The results of computations were also compared with experimental measurements of temperature and seepage flow rates made on a laboratory model of a soil freezing system. O'Neill and Albert [13] numerically investigated solidification of porous media in the presence of natural convection using a finite element method. Weaver and Viskanta [14, 15] studied the freezing of a liquid-saturated porous medium in cylindrical and rectangular enclosures. The agreement between numerical model predictions considering conduction only and experimental data was good for a water–glass bead system; however, for a water–aluminum bead system there were significant discrepancies between data and predictions due to an unreliable effective thermal conductivity model of the porous media.

This paper reports on the experimental and numerical study of the freezing of a water–glass bead system. The measured frozen fractions, temperatures, and solidification front locations are compared with one-dimensional model predictions considering conduction as the only mode of heat transfer in both the liquid and the solid. Experimental data are also reported for freezing of superheated water in the presence of natural convection flow in the porous medium.

EXPERIMENTS

Test cell

Solidification experiments were performed in a rectangular test cell with inner dimensions of 205 mm in

NOMENCLATURE

A	aspect ratio, H/L
c	specific heat [J kg^{-1} K^{-1}]
d	bead diameter [mm]
D	depth of cavity [m]
g	gravitational acceleration [m s^{-2}]
h'	volumetric interphase heat transfer conductance or coefficient [W m^{-3} K^{-1}]
Δh_f	latent heat of fusion [J kg^{-1}]
H	height of liquid level [m]
k	thermal conductivity [W m^{-1} K^{-1}]
K	permeability [m^2]
L	length of cavity
Ra^*	Rayleigh number, $g\beta_l(T_h-T_c)KL/(\nu_l\alpha_l)$
s	interface position from cold wall [m]
Ste	Stefan number, $c_l(T_h-T_c)/\Delta h_f$
Ste^*	initial Stefan number, $c_l(T_i-T_c)/\Delta h_f$
t	time [s]
T	temperature [K]
V	volume [m^3]
x	horizontal distance from cold wall, see Fig. 1 [m]
y	vertical coordinate, see Fig. 1 [m].

Greek symbols

α	thermal diffusivity, $k_l/(\rho_l c_l)$ [m^2 s^{-1}]
β	coefficient of thermal expansion [K^{-1}]
γ	dimensionless volumetric heat transfer conductance or coefficient, $(h'L^2/(\rho_p c_p \alpha_l))$
ζ	dimensionless interface position, s/L
η	dimensionless vertical coordinate, y/L
θ	dimensionless temperature, $(T-T_c)/(T_h-T_c)$
ν	kinematic viscosity [m s^{-2}]
ξ	dimensionless horizontal coordinate, x/L
τ	dimensionless time, $t\alpha_l/L^2$
ϕ	porosity.

Subscripts

c	cold
eff	effective
f	fusion
h	hot
i	initial
l	liquid
p	porous matrix
s	solid
w	water.

Superscript

~	properties for the non-equilibrium model.

length, 203 mm in height and 127 mm in width. The top, bottom, front and back sides were made of Plexiglas (12.5 mm thick). Two Plexiglas plates separated by a 6 mm air gap were used on the front and back of the test cell to minimize the effect of heat losses and condensation of moisture. A 7.5 mm wide and 172 mm long slot was cut in the top plate. The test cell was filled with water and glass beads through this opening. A lid fit snugly into this slot. Two 11 mm diameter holes were cut in this lid to bring out the thermocouple wires to allow excess water to be displaced out of the cell as freezing progresses. A 19 mm diameter, tygon tube covered one of the holes. The other end of the tube was connected to a burette to measure the amount of water displaced during the freezing process. The other hole was covered with a rubber stopper. The thermocouple wires were passed through a small hole at the center of the stopper. All the holes were made watertight.

Two copper heat exchangers with milled passages for flow of coolant constituted the left and right endwalls of the test cell. The flow passages inside the heat along the surface of the heat exchanger was within ± 0.2°C. Six thermocouples were placed along the surface of the heat exchangers to check the uniformity of the temperature along their faces. The entire test cell was covered with 50 mm thick Styrofoam on all sides. The test cell was placed on an iron plate fitted with leveling screws.

A thermocouple rake with 21 copper–constantan thermocouples was supported on two half rings epoxyed on to the surface of the heat exchangers. The rake was located at midheight and along the centerplane of the test cell. For experiments with natural convection present in the liquid, two rakes at one-third and two-thirds height from the bottom were used. The temperatures were recorded using a datalogger connected to a VAX microcomputer.

Test materials and procedure

Spherical soda lime glass beads of average diameters 2.85, 6 and 12 mm constituted the porous media. The properties used for the numerical study were for a soda lime glass with a chemical composition as close as could be obtained to the chemical composition of the beads used in this study.

The test cell was filled with glass beads with rakes kept in position. Once distilled, degasified water was carefully siphoned into the test cell without introducing air bubbles into the system. One end of the tygon tube was inserted into one of the holes on the top lid and the other was connected to a burette. The tygon tube was filled with distilled water and the initial level of water in the burette was noted. A mixture of

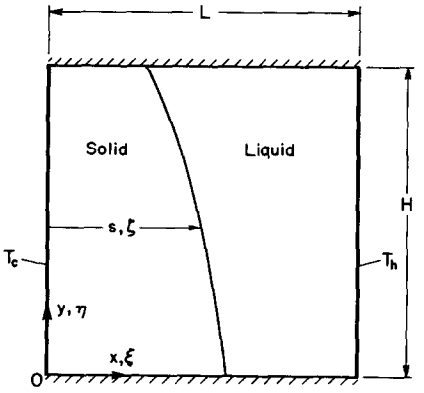

FIG. 1. Schematic of the test cell.

ethyl alcohol and water was circulated through the two heat exchangers from two constant temperature baths.

Experiments were performed with the liquid close to the fusion and significantly above the fusion temperatures. In the later series of experiments natural convection was present in the porous medium when one of the walls was maintained above 0°C. Since the test cell was very wide, even after two days, the water in the entire cell could not be cooled, for example, to 0°C. The freezing was initiated by switching one of the constant temperature baths to a third one that was already precooled, separately to the desired temperature. Temperature measurements were automatically recorded at given intervals of time by the datalogger. The water level in the burette was also recorded at different time intervals. The presence of natural convection in the unfrozen porous media and the flow structure were observed in parallel flow visualization experiments.

ANALYSIS

The physical system modeled consists of a rectangular cavity with two vertical walls maintained at two different temperatures and the top and the bottom surfaces insulated. The cavity is filled with a mixture of water and uniform size spheres (porous matrix). At $t = 0$, the system is at a uniform temperature greater than or equal to the fusion temperature, $T_i > T_f$, of the liquid. At time, $t > 0$, a uniform temperature less than the fusion temperature is imposed on the left wall. Freezing is initiated at this wall and the interface moves from left to right (Fig. 1). The following simplifying assumptions are made in the analysis.

(1) The porous medium is isotropic, homogeneous and has uniform porosity.

(2) All the thermophysical properties are independent of temperature.

(3) The volume change due to freezing is negligible.

(4) Natural convection is absent. Hence, conduction is the only mode of heat transfer both in the solid and the liquid regions.

(5) The phase change medium (PCM) has a definite fusion temperature.

(6) There is no thermal equilibrium between the PCM and the porous matrix. This may be the case when the porous matrix has a much larger thermal conductivity than the PCM, and the interphase heat transfer must be properly accounted for.

Based on the above assumptions, the one-dimensional non-equilibrium model equations in dimensionless form for the porous matrix and the frozen PCM are

$$(1-\phi)\frac{\partial\theta_p}{\partial\tau} = \left(\frac{\tilde{\alpha}_p}{\tilde{\alpha}_l}\right)\frac{\partial^2\theta_p}{\partial\xi^2} + \gamma(\theta_s - \theta_p) \tag{1}$$

$$\phi\frac{\partial\theta_s}{\partial\tau} = \left(\frac{\tilde{\alpha}_s}{\tilde{\alpha}_l}\right)\frac{\partial^2\theta_s}{\partial\xi^2} + \frac{(\rho c)_p}{(\rho c)_s}\gamma(\theta_p - \theta_s). \tag{2}$$

The equations for the porous matrix–liquid PCM are obtained by replacing the subscript 's' by 'l'. It should be mentioned that $\tilde{\alpha}_p$, $\tilde{\alpha}_s$, and $\tilde{\alpha}_l$ (i.e. thermal conductivities $\tilde{k}_p$, $\tilde{k}_s$ and $\tilde{k}_l$) are effective properties that take into account the dispersed structure of the solid matrix (i.e. the effect of hydrodynamic dispersion resulting from the flow). The interphase heat transfer between the matrix and the solid or liquid PCM depends on the characteristics of both phases, on the nature of the porous matrix (and on the fluid velocity if convection is present)

$$\frac{\phi\rho_s}{\rho_l(Ste)}\frac{\partial\zeta}{\partial\tau} = \left(\frac{\tilde{k}_s}{\tilde{k}_l}\right)\frac{\partial\theta_s}{\partial\xi} - \frac{\partial\theta_l}{\partial\xi}. \tag{3}$$

The temperature at the solidification front is continuous and is equal to the fusion temperature of the PCM. The left (cold) and the right (hot) walls are maintained at prescribed temperatures.

Method of solution

The numerical solution of phase change problems poses complications due to the motion of the solidification front. The location of the front is not known *a priori*, and the size and shape of the solid and liquid domains vary with time. Additionally, there is a discontinuity in the temperature gradient at the front. The equations were discretized over each control volume [16] using an implicit finite difference scheme. Two different approaches were considered for modeling the moving front: (1) keep the total number of nodes in each region fixed and at each time step as the front moves and the domain size varies, redistribute the grid system, or (2) keep the grid distribution fixed and track the front motion as it progresses from one node to the other.

In the former approach, the interpolation or extrapolation necessary to calculate the temperatures of the new nodal points, reduces the accuracy and increases the computer time. Hence, though the latter approach presents the problem of dealing with a varying number of grids at each time step, it was chosen.

A node is specified on the interface. To eliminate the inaccuracy introduced by interpolation or extrapolation [17], unequal spacing (which varies with time) in the computational grid on both sides of the interface is employed.

Finite differencing of the interfacial energy balance requires an accurate approximation for the first derivative of temperature using the unequal spacing at the interface. By twice differentiating a second-order polynomial and solving for the first derivative (e.g. liquid side of the interface), a suitable formula was derived which uses the interface node and two adjacent nodes on the liquid side of the interface. The calculations are started by assuming a very thin ice layer to be present at $t = 0$.

The grid independence of the solution was checked by performing calculations for different grids [18]. The equations were also solved for freezing of pure water without any beads ($\phi = 1.0$), and the results compared with that of Stefan's solution (for saturated PCM) and Neumann's solution (for superheated PCM). The good agreement between them established confidence in the model.

RESULTS AND DISCUSSION

Water at saturated conditions

The two heat exchangers were maintained at temperatures as close to 0°C as possible, and the system was allowed to cool for about 24–36 h before each experiment. Due to the large width of the cell, the average initial temperature was in the range of 1–2°C. It is believed that the natural convection caused by this small superheat, especially in a porous media under these conditions is negligible. As a consequence of the finite heat capacity, an instantaneous (step change) in the heat exchanger temperature is not possible. A finite time is needed before the exchangers attain constant steady-state values.

Freezing of the distilled, deionized water–aluminum ball system was unsuccessful and had to be abandoned. Water supercooled greatly, and it was not possible to use measured temperatures to locate the solidification front. Since the system is also highly reflecting, photography could not be used also. A number of experiments with three different glass diameter beads were conducted successfully and are reported here. For space limitations, only a few of them are discussed in this paper. Additional results are presented elsewhere [18]. The experimental conditions are given in Table 1. The measured data are compared with the values predicted by the model. In this comparison, the variation of cold wall temperature with time and the initial temperatures must be taken into consideration. Hence, the numerical model used the measured cold wall temperatures and the initial temperature variations with time as input data. All the properties for ice, water and the beads were evaluated at the fusion temperature of 0°C. The permeability is calculated using the Kozeny–Carman equation [9].

Table 1. Summary of experimental conditions (natural convection is absent)

Exp.	d (mm)	T_c (°C) (steady)	ϕ	$K \times 10^{-9}$ (m^2)
S1	12.5	−5.7	0.399	157
S2	6.0	−5.7	0.360	23.4
S3	6.0	−8.9	0.360	23.4
S4	2.85	−7.11	0.345	4.44

From Table 1 it is seen that the porosity ϕ varies with bead size. For a system of infinite volume, randomly packed with uniform size spheres, the porosity is constant and is independent of the bead size [19]. Since the test cells used in the experiments are finite in size, there is a considerable variation of porosity near the walls [20], especially with the larger size beads. With 2.85 mm beads, the packing is closest and the porosity is close to the theoretically expected value for random bead packing.

Initial simulations of freezing of water–glass beads and water–aluminum balls systems were performed by assuming that $\tilde{k}_p = k_p$, $\tilde{k}_s = k_s$, $\tilde{k}_l = k_l$ and arbitrary values of dimensionless interphase heat transfer conductance γ to model both systems. The value of the conductance was found to have very little effect on the interphase heat transfer and equilibrium was attained very quickly. A similar observation was recently made by Sugawara *et al.* [21] in their study of the freezing of a water-saturated horizontal porous layer. Hence, the calculations reported in this paper are based on the equilibrium model, $T_p = T_f$, for which the second term on the right-hand side of equations (1) and (2) vanishes. This idealization is justified well for the water–glass beads system because the difference between the thermal conductivities of the porous matrix and the PCM is small.

Under thermal equilibrium conditions, the effective thermophysical properties of the porous media are calculated using the volumetric averaging technique [8]. Thus, the effective thermal capacitance is given by

$$(\rho c)_{sp} = \phi(\rho c)_s + (1-\phi)(\rho c)_p. \tag{4}$$

Replacing the properties of the solid by those of the liquid in the above equation, the effective thermal capacitance of the unfrozen porous media can be calculated. Different models [9, 22] have been proposed for determining the effective thermal conductivity of the porous media. Veinberg [23] developed a model which is claimed to be universally applicable for randomly distributed spherical inclusions in a medium. Accordingly, the effective thermal conductivity is given by

$$k_{sp} + \frac{\phi(k_p - k_s)}{k_s^{1/3}} k_{sp}^{1/3} - k_p = 0. \tag{5}$$

Sensitivity studies of the different models have been conducted [14], and it was found that for a water–glass bead system, Veinberg's model produced the closest

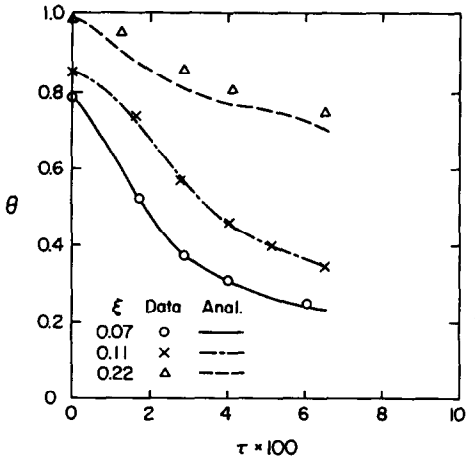

FIG. 2. Comparison of predicted and measured temperatures for experiment S2 ($d = 6$ mm, $\phi = 0.36$, no convection).

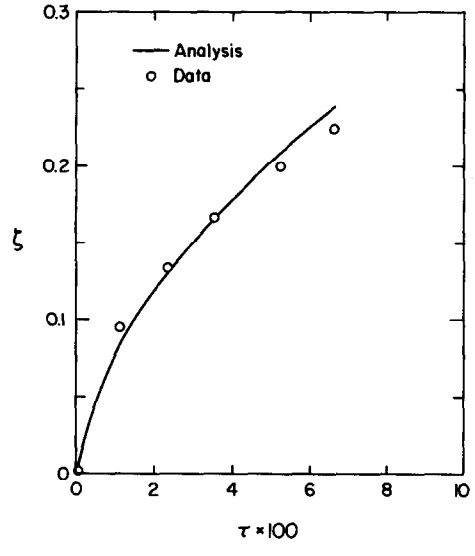

FIG. 3. Comparison of predicted and measured solidified layer thickness for experiment S2 ($d = 6$ mm, $\phi = 0.336$, no convection).

agreement between the experimental data and the predictions.

Temperature distribution

Figure 2 shows the comparison between the measured and predicted dimensionless temperatures at three different locations as a function of time for experiment S2. The overall agreement between the data and the predictions is good. The model underpredicts the temperatures for the location, $\xi = 0.22$; however, this discrepancy is small (about 5% of the total temperature difference across the test cell) and is within experimental accuracy. The comparison of the dimensionless solidification front position as a function of time is presented in Fig. 3. The front is said to have crossed a thermocouple when it recorded a temperature of 0°C. At later times, the model slightly overpredicts the freezing rate. With the passage of time the rate of freezing decreases due to the increasing

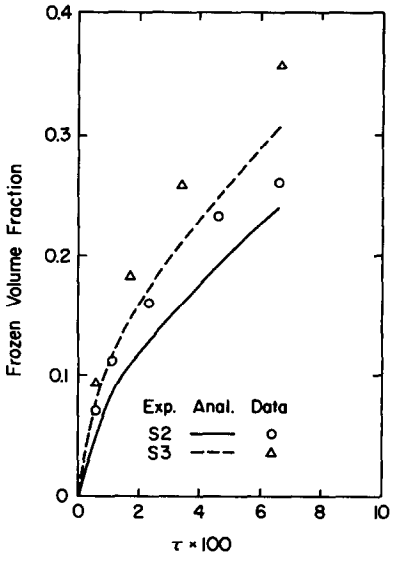

FIG. 4. Comparison of predicted and measured frozen volume fractions for experiment S2 ($d = 6$ mm, $\phi = 0.36$, no convection).

thermal resistance offered by the ice–porous media matrix formed on the wall. The frequency of data acquisition was reduced, from that at earlier times, to avoid storing a very large amount of data. Hence, the possible error introduced in interpolation to locate the solidification front may have been larger at later times. In fact, if all the water was frozen (in the experiments the large width of the test cell prevented it) then near the completion of the freezing process the data would reveal a higher rate of freezing than the analysis [14].

Solidification front position

Since the density of ice is approximately 10% lower than that of water, 10% of the original mass of water is displaced out of the system during freezing. This is not accounted for in the model. Since the heat transfer is one-dimensional, the frozen volume fraction as predicted by the model is equal to the dimensionless solidification front location. Experimentally, it is calculated from the water displacement measurements as:

volume of ice formed

$$V_{ice} = DHs\phi;$$

volume of water corresponding to the volume of ice

$$V_w = V_{ice}(\rho_{ice}/\rho_w);$$

volume of water displaced

$$V_{disp} = V_{ice} - V_w = V_{ice}\left(1 - \frac{\rho_{ice}}{\rho_w}\right);$$

frozen volume fraction

$$\frac{V_{ice}}{V_{cell}} = \frac{V_{disp}}{V_{cell}\left(1 - \frac{\rho_{ice}}{\rho_w}\right)}. \quad (6)$$

A comparison between the predictions and the data for the volume fraction (Fig. 4) showed that the model

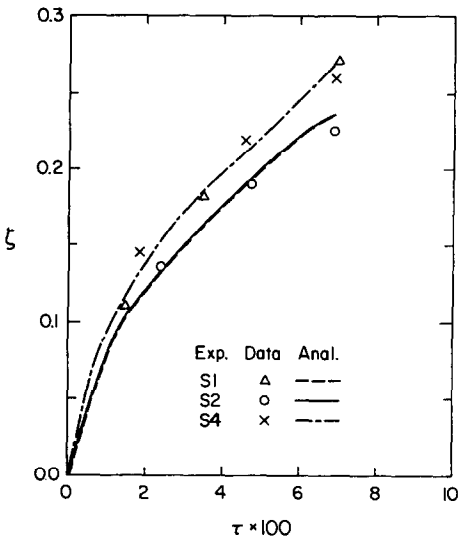

FIG. 5. Effect of bead diameter on the rate of freezing (experiments S1, S2 and S4, no convection).

always underpredicts the freezing rate. The most probable reasons for the discrepancy may have been entrapment of air in the test cell during the filling process of water and/or absorption of air at the surface of the glass beads and the release of air during freezing. This release causes more water to be displaced out of the test cell than predicted by the model. The porosity at the walls is close to unity and varies exponentially for a region of about three bead diameters [20]. Hence, according to equation (6), as freezing progresses more water is displaced out of the system and the error increases. It is speculated that a combination of the two reasons causes the discrepancy between data and predictions. This figure also shows the effect of wall temperature on the rate of freezing. As expected, with lower wall temperatures, the freezing proceeds at a faster rate. This agrees with the published results for freezing of porous media in a cylindrical cavity [14].

Figure 5 shows the effect of bead size on the freezing process. Experiments S1 and S2 have the same cold wall temperature at steady state, but S4 has a lower wall temperature. Yet, they could be compared to examine the influence of the bead size. The numerical predictions for experiments S1 and S2 overlap each other. The bead size does not directly appear in the governing equations. Only the variation in porosity (for reasons mentioned earlier) with bead size influences the effective properties and thus indirectly the rate of freezing. In the above experiments, the influence of this difference is small, and hence the predicted curves overlap. But the experimental data points do not overlap.

The figure also shows the rate of freezing for 12.5 mm beads (experiment S1) to be higher than that for 6 mm (experiment S2) beads, though the cold wall temperatures were the same. The porosity (hence the amount of water to be frozen) is higher for the larger size beads. The average initial temperature for experiment S1 was 0.82°C while that for S2 was 2.03°C. Hence, even though the porosity is higher, the decrease in superheat causes the rate of freezing to be faster for the 12.5 mm beads.

Freezing of initially superheated water

The superheat of water induces natural convection flow during the freezing process. The process is influenced by the flow as observed visually by the curved shape of the solidification front and contrasted against the nearly plane interface seen when water was not superheated. Flow visualization during freezing of a porous media was not possible. Hence, the flow patterns under thermal conditions close to those prevailing during freezing were visualized [24].

The shape of the interface could not be photographed due to the scattering of light by the glass beads and the small difference between the refractive indices of water and beads. Hence, interface shape was deduced from direct observations (when possible) and temperature measurements. Two thermocouple rakes, placed at one-third and two-thirds height from the bottom, recorded the temperatures at two vertical locations. The use of additional rakes was avoided to minimize the disturbance introduced to the flow.

A number of experiments, with varying amounts of superheat, different wall temperatures and with different size glass beads were conducted. Each experiment lasted for 24 h. Only the conditions for those experiments discussed in this paper are presented in Table 2. In this section, only the experimental results are presented. The comparison with a numerical model that considers the density inversion of water and natural convection in liquid will be reported in the near future [18].

Temperature distributions

The temperature variations at different times as recorded by the two thermocouple rakes for experiment N1 are presented in Fig. 6. The temperature difference between the solidification front (or interface) and the hot wall drives the natural convection flow in the liquid. The thermocouple nearest to the cold wall is at a distance of 1.5 cm and the farthest one is at a distance of 17.0 cm. Even after 1 h into the freezing process, the water in the region about 5 cm away from hot wall remains at the initial temperature indicating very weak flow.

For this experiment, the temperature difference driving the flow is about 6°C; therefore, the currents are not as strong as in experiment N2 (explained later). The temperature distributions reveal that the rate of freezing along the top rake to be faster than that along the bottom rake. This is in contrast to that observed in the freezing of other common liquids [25]. Due to the density inversion of water, there are two convective cells [24]: a counter-clockwise rotating cell driven by 0–4°C and a clockwise flow driven by 4–6°C temperature ranges. The counter-clockwise flow

Table 2. Summary of experimental conditions (with natural convection, $A = 0.75$)

Exp.	d (mm)	T_i (°C) (average)	T_c (°C) (steady)	ϕ	$K \times 10^{-9}$ (m^2)	Ste^*	Ra^* ($\times 10^{-5}$)
N1	12.5	6.1	−6.2	0.412	180.6	0.156	56.90
N2	12.5	12.4	−15.8	0.412	180.6	0.358	130.46
N3	6.0	6.6	−7.2	0.396	35.02	0.175	12.38
N4	6.0	12.5	−13.4	0.396	35.02	0.328	23.23
N5	6.0	18.5	−11.9	0.396	35.02	0.385	27.27
N6	2.85	12.9	−13.9	0.377	6.41	0.336	4.4

is stronger. The water near the interface and the hot wall rises. As the water flows upwards along the interface, it is cooled; therefore, the freezing is faster at the top than at the bottom. For ordinary liquids the fluid is cooled as it descends along the interface, and hence it freezes faster at the bottom than at the top of the wall.

From the figure it is evident that the temperature gradients in the liquid are smaller at the bottom than at the top. Hence, as seen from the interface energy balance (equation (3)), the smaller gradients cause freezing at the top to be faster than at the bottom. With the progress of freezing this difference in the temperature gradients and hence the rate of freezing increases.

The time–temperature traces for experiment N2 are presented in Fig. 7. They reveal stronger convective flow than in experiment N1, and the freezing at the bottom is faster than at the top. In this experiment, the average initial superheat is 12.4°C. The counterclockwise flow in the region 0–4°C is not as strong as the clockwise flow in the region 4–12°C. This flow structure was observed in flow visualization studies in water saturated porous media under temperature conditions close to those of the present experiments [24]. As the driving temperature potential for the two flows differ by a factor of two, it could be roughly interpreted that their strengths also differ by a factor of two. Consequently, the freezing at the bottom is faster as in ordinary liquids.

The time–temperature traces for selected thermocouples along the two rakes are presented in Fig. 8. The time taken for the interface to cross a particular thermocouple can be found readily from this figure. The time taken to freeze 1.5 cm at the top and bottom are 47.5 and 22.5 min, respectively, indicating the influence of convection on freezing at very early times in the experiment.

Solid/liquid interface position

The effect of Stefan number (based on the initial average temperature) on the rate of freezing is shown in Fig. 9. The interface positions for experiments N3, N4 and N5 (6 mm beads) are compared in this figure. At the end of the 24 h period, only those thermocouples that recorded 0°C are used for plotting. The temperature measurements for experiment N3 did not reveal any noticeable difference between the two rakes. Thus, this provides evidence that there was hardly any natural convection flow present in the system. This evidence is corroborated by the results of others [14]. With a decrease in the bead size, the permeability decreases (the permeability is directly proportional to the square of the bead diameter) considerably. This is in contrast to that seen in experiment N1 for the same superheat, i.e. Stefan number. For

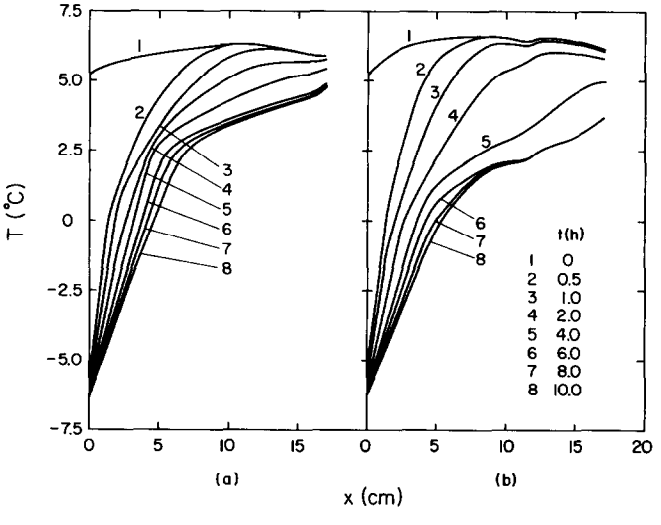

FIG. 6. Temperature distribution at different times for experiment N1 ($d = 12.5$ mm, $\phi = 0.412$, $Ste^* = 0.156$): (a) bottom rake, $\eta = 0.333$; (b) top rake, $\eta = 0.667$.

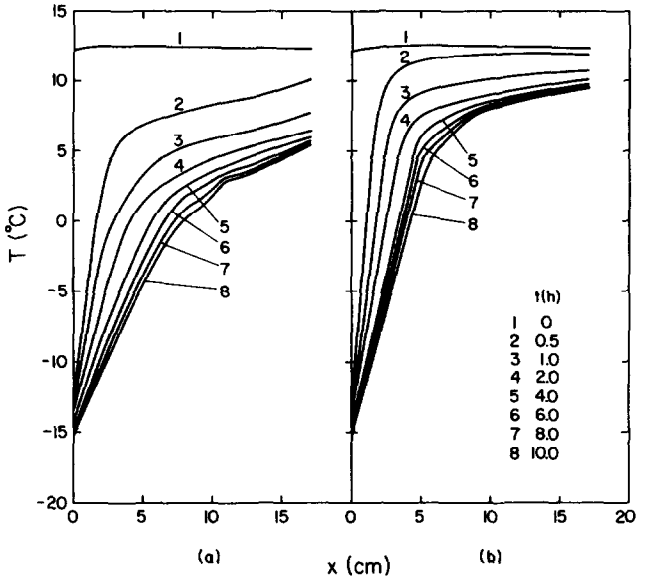

FIG. 7. Temperature distribution at different times for experiment N2 ($d = 12.5$ mm, $\phi = 0.412$, $Ste = 0.358$): (a) bottom rake, $\eta = 0.333$; (b) top rake, $\eta = 0.667$.

experiments N4 and N6, the effects of convection were significant and freezing at the bottom was faster. In experiment N5, due to a power failure, the data acquisition was interrupted. The calculation of interface position at later times, require interpolations over large time intervals (possibly introducing big errors) and hence are not plotted.

Figure 10 shows the effect of bead size on the rate of freezing for experiments N2, N4 and N6. In all the experiments, the freezing at the bottom rake was faster than that at the top. The influence of convection increases with time as evidenced by the widening gap between the two curves for any experiment. The average superheat was about 12.5°C for experiments N2, N4 and N6. The possible convective flow in the 0–4°C region is practically overpowered by the flow in the 4–12.5°C region. Hence, freezing proceeds faster at the bottom as in ordinary liquids. Also, for experiment N6, the influence of convection is not as prominent as in other experiments, and the duration of the conduction dominated freezing regime is the longest. As mentioned earlier, this is expected due to the low permeability and high resistance offered to buoyancy driven convection.

Experiments (not discussed here) showed that a superheat of 6°C produced very little convective flow for 6 mm beads and no flow for 2.85 mm beads [18]. With a superheat of 18°C, there was very little freezing

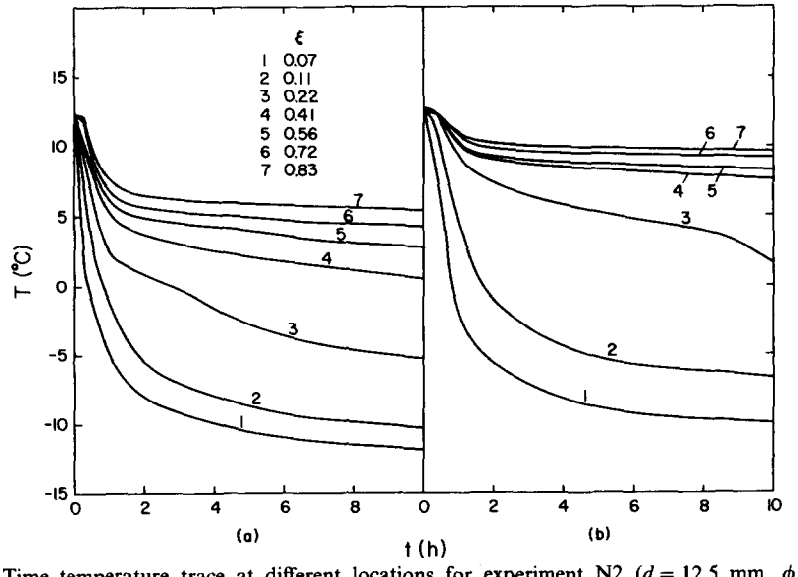

FIG. 8. Time–temperature trace at different locations for experiment N2 ($d = 12.5$ mm, $\phi = 0.412$, $Ste^* = 0.358$): (a) bottom rake, $\eta = 0.333$; (b) top rake, $\eta = 0.667$.

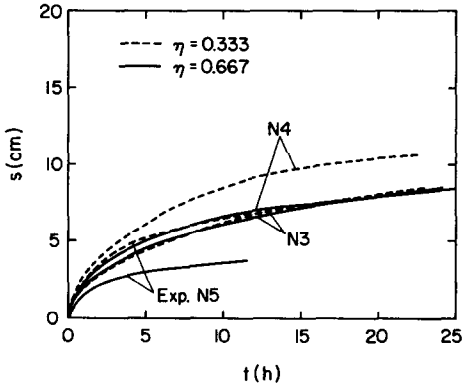

FIG. 9. Effect of initial Stefan number (Ste^*) on the rate of freezing for experiments N3, N4 and N5 ($d = 6$ mm, $\phi = 0.396$).

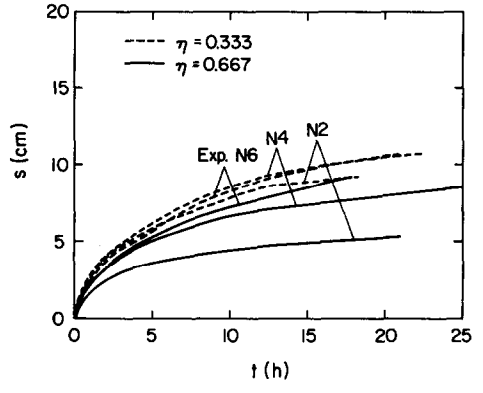

FIG. 10. Effect of bead size on the rate of freezing for experiments N2 ($d = 12.5$ mm), N4 ($d = 6$ mm) and N6 ($d = 2.85$ mm).

with 12.5 mm beads at an initial superheat of 6°C due to the strong convective flow.

CONCLUSIONS

An experimental and numerical study of freezing of water saturated porous media has been undertaken. The one-dimensional model considering conduction alone in both the solid and liquid phases predicted well the temperature distribution and the rates of freezing even when the liquid superheat was about 2°C. The measured and predicted frozen volume fractions showed the worst comparison, possibly due to the release of entrapped air and the variation of porosity near the wall and the thermocouple rakes.

When the superheat is sufficiently large to induce buoyancy driven convective flow, the solidification front is no longer planar. For 12.5 mm glass beads at an initial superheat of 6°C due to the density inversion of water, the buoyancy induced currents produced faster freezing in the upper part than in the lower part of the wall. But for the same superheat, there was hardly any convection present with 2.85 mm beads. The superheat of 12°C and higher overpowered the effect of density inversion, and the freezing was faster at the bottom of the wall, like in ordinary liquids.

There is a need for flow visualization and diagnostics for temperature and solidification front position measurement in porous media both in the absence and in the presence of phase change. There is also a need for efficient numerical algorithms for solving the model equations for two-dimensional solid/liquid phase change of porous media in the presence of natural convection.

Acknowledgements—The work reported in this paper was supported, in part, by the Heat Transfer Program of the National Science Foundation under Grant No. CBT-8313573.

REFERENCES

1. ME Staff, Seasonal thermal energy storage, *Mech. Engng* **105**(3), 28–34 (1983).
2. F. V. Albin, S. Srinivasamurthy and M. V. Krishnamurthy, Analysis of the food freeze drying process with predetermined surface temperature variation. In *Drying '82* (Edited by A. S. Mizumdar), pp. 151–156. Hemisphere, Washington, DC (1982).
3. V. J. Lunardini, *Heat Transfer in Cold Climates*, Van Nostrand Reinhold, New York (1981).
4. F. J. Sanger, Ground freezing in construction, *ASCE Mech. Found. Div.* **94**, 131–158 (1968).
5. P. D. Metz, A simple computer program to model three-dimensional underground heat flow with realistic boundary conditions, *ASME J. Solar Energy Engng* **105**, 42–49 (1983).
6. O. Svec, L. E. Goodrich and J. H. L. Planar, Heat transfer characteristics of inground heat exchangers, *J. Energy Res.* **7**, 263–278 (1983).
7. W. Aung and Y. Yener, Research directions in natural convection. In *Natural Convection: Fundamentals and Applications* (Edited by S. Kakac, W. Aung and R. Viskanta), pp. 1155–1171. Hemisphere, Washington, DC (1986).
8. P. Cheng, Heat transfer in geothermal systems. In *Advances in Heat Transfer* (Edited by T. F. Irvine, Jr. and J. P. Hartnett), Vol. 14, pp. 1–106. Academic Press, New York (1978).
9. M. A. Combarnous and S. A. Bories, Hydrothermal convection in saturated porous media. In *Advances in Hydroscience*, Vol. 10, pp. 231–307. Academic Press, New York (1975).
10. M. E. Goldstein and R. L. Reid, Effect of fluid flow on freezing and thawing of saturated porous media, *Proc. R. Soc. London* **A364**, 45–73 (1978).
11. H. T. Hashemi and C. M. Sliepcevich, Effect of seepage stream and artificial soil freezing, *ASCE Mech. Found. Div.* **99**, 267–289 (1973).
12. P. E. Frivik and G. Comini, Seepage and heat flow in soil freezing, *ASME J. Heat Transfer* **104**, 323–328 (1982).
13. K. O'Neill and M. R. Albert, Computation of porous media natural convection flow and phase change. In *Finite Elements in Water Resources* (Edited by J. P. Laible, C. A. Brebbia, W. Gray and G. Pinder), pp. 213–229. Springer, Berlin (1984).
14. J. A. Weaver and R. Viskanta, Freezing of liquid-saturated porous media, *ASME J. Heat Transfer* **108**, 654–659 (1986).
15. J. A. Weaver and R. Viskanta, Freezing of water saturated porous media in a rectangular cavity, *Int. Commun. Heat Mass Transfer* **13**, 245–252 (1986).
16. S. V. Patankar, *Numerical Heat Transfer and Fluid Flow*. McGraw-Hill, New York (1980).

17. W. D. Murray and F. Landis, Numerical and machine solutions of transient heat conduction problems involving melting or freezing, *ASME J. Heat Transfer* **81,** 106–112 (1959).
18. S. Chellaiah, An experimental and numerical study of freezing and melting of liquid saturated porous media, Ph.D. Thesis, Purdue University (in preparation).
19. R. F. Benenati and C. B. Brosilow, Void fraction distribution in beds of spheres, *A.I.Ch.E. Jl* **8,** 359 (1962).
20. B. C. Chandrasekara and D. Vortmeyer, Flow model for velocity distribution in fixed porous beds under isothermal conditions, *Wärme- und Stoffübertr.* **12,** 105–111 (1979).
21. M. Sugawara, H. Inaba and N. Seki, Effect of maximum density of water on freezing of water-saturated horizontal porous layer, *ASME J. Heat Transfer* (1988), in press.
22. O. Farouki, Evaluation of methods for calculating soil thermal conductivity, Cold-region Research and Engineering Laboratory Report 82-8, March (1982).
23. A. K. Veinberg, Permeability, electrical conductivity, dielectric constant and thermal conductivity of a medium with spherical and ellipsoidal inclusions, *Sov. Phys. Dokl.* **11,** 593–595 (1967).
24. S. Chellaiah and R. Viskanta, Natural convection flow visualization in porous media, *Int. Commun. Heat Mass Transfer* **14,** 607–616 (1987).
25. R. Viskanta, Phase change heat transfer. In *Solar Heat Storage: Latent Heat Materials* (Edited by G. A. Lane), Vol. 1, pp. 153–222. CRC Press, Boca Raton, Florida (1983).

GEL DE LIQUIDE SATURANT ET SURCHAUFFE DANS DES MILIEUX POREUX

Résumé—On étudie expérimentalement le gel d'un liquide saturé et surchauffé dans un milieu poreux contenu dans une cellule rectangulaire. De l'eau et des billes de verre de différents diamètres constituent respectivement le liquide et les milieux poreux. On considère les effets des différentes tailles de billes de verre, de la différence de température imposée et de la surchauffe du liquide. Un modèle monodimensionnel basé sur la conduction est utilisé pour examiner les effets de non équilibre. Ceux-ci sont de peu d'importance pour des billes d'aluminium ou des billes de verre. Pour l'eau à la température initiale du gel, les prédictions du modèle s'accordent bien avec la température expérimentale et les données du déplacement du front de solidification. Quand la surchauffe est suffisamment grande pour induire un écoulement de convection naturelle, la vitesse locale de gel varie avec la position verticale le long du mur froid. Pour de faibles surchauffes, à cause de l'inversion de densité de l'eau, la vitesse de gel au sommet est plus élevée qu'à la base; néanmoins pour de grandes surchauffes, la vitesse de gel près de la base est plus élevée que pour le gel des liquide ordinaires.

DAS GEFRIEREN VON GESÄTTIGTER UND ÜBERHITZTER FLÜSSIGKEIT IN PORÖSEN MEDIEN

Zusammenfassung—Das Gefrieren gesättigter und überhitzter flüssigkeitsgefüllter poröser Medien in einer rechteckigen Testzelle wurde experimentell untersucht. Das Korngerüst des porösen Mediums bestand aus Glaskugeln unterschiedlichen Durchmessers, die Flüssigkeit war Wasser. Die Einflüsse der Größe der Glaskugeln, der aufgeprägten Temperaturdifferenz und der Flüssigkeitsüberhitzung wurden untersucht. Ein eindimensionales Modell auf der Basis der Wärmeleitung wurde zur Untersuchung der Nicht-Gleichgewichtseffekte verwendet. Diese Effekte hatten keinen Einfluß bei Systemen aus Wasser und Aluminiumkugeln sowie aus Wasser und Glaskugeln. Zu Beginn des Gefriervorgangs stimmen die Berechnungen gut mit der gemessenen Temperatur und der Position der Erstarrungsgrenze überein. Solange die Überhitzung genügend groß ist, um eine Auftriebsströmung zu erzeugen, hängen die lokalen Gefrierraten von der vertikalen Position an der gekühlten Wand ab. Bei kleiner Überhitzung war die gefrorene Wassermenge wegen des Dichtemaximums von Wasser oben größer als am Boden; bei großen Überhitzungen war die gefrorene Menge am Boden größer als bei gewöhnlichen Flüssigkeiten.

ЗАМЕРЗАНИЕ НАСЫЩЕННОЙ ПЕРЕГРЕТОЙ ЖИДКОСТИ В ПОРИСТЫХ СРЕДАХ

Аннотация—Экспериментально изучено замерзание жидкости в насыщенных перегретых пористых средах, заключенных в прямоугольной опытной ячейке. Жидкую и пористую среды составляют, соответственно, вода и стеклянные шарики различных диаметров. Изучалось влияние размеров стеклянных шариков, разности температур и перегрева жидкости. Для определения влияния неравновесных эффектов использовалась одномерная модель теплопроводности. Найдено, что эффекты не существенны как для систем вода–алюминиевые шарики, так и для систем вода–стеклянные шарики. для воды, имеющей начальную температуру замерзания, расчеты с помощью данной модели хорошо согласуются с экспериментальными данными по температуре и положению фронта затвердевания. В сдучае, когда перегрев достаточен для того, чтобы привести к конвективному течению, вызванному подъемными силами, локальные скорости замерзания изменялись с изменением положения по вертикали вдоль охлажденной стенки. Для низкого перегрева из-за инверсии плотности воды интенсивность замерзания наверху была выше, чем внизу, однако для большого перегрева, скорость замерзания у дна была выше, как в случае замерзания обычных жидкостей.